# ALMA Memo 503
# Antenna position determination: Observational methods and atmospheric limits

John Conway

Onsala Space Observatory, Sweden

jconway@oso.chalmers.se

September 2nd, 2004

**Abstract**

We discuss the accuracy to which ALMA antenna relative positions can be determined via astronomical observations of phase and delay toward multiple strong calibrators. We show that delay induced phase gradients across the bandpass can be used to resolve turn ambiguities so that accurate delays can estimated from the phase. At low frequencies this demands only modest stability of the bandpass phase. For this and other reasons we argue that 90GHz is the best frequency for position calibration observations. The proposed specification for short time instrumental phase stability is adequate for antenna position determination. We discuss in detail the effect of the wet troposphere and derive how position errors scale with baseline length in the case of single-baseline calibration. We then generalise to a full calibration of the whole array. It is found that the resulting position errors between two antennas is the same as if these two antennas participated in there own single baseline calibration. We find that because of the geometry and the need to solve for instrumental phase that even on short baselines the rms error on the vertical or z-component is twice as large as for the x and y components. In addition for $> 1$km baselines while the x and y rms errors rapidly saturate the z components rms errors continue to increase. Some uncertainly in estimating errors on long baselines comes from our lack of knowledge of the outer scale of turbulence at the site. The effects of systematic gradients in the zenith wet or dry delay and methods of calibration are briefly considered.

We propose that when in the intermediate 'zoom' array configurations an initial calibration of the moved antennas is made in late afternoon lasting 30minutes. Later in the early hours of the morning, when phase stability is best, we propose a 30 - 60 minute calibration of the whole array. Because of the need to apply phase corrections for antenna positions retro-actively even continuum data should always be stored in spectral line mode with channel widths $< 1$GHz. Final pipelining for the highest dynamic range imaging may have to wait for up to 12 hours until good antenna positions are obtained. With good 'a priori' positioning of antennas on pads and/or the acceptance of delayed pipelining as the norm after reconfiguration the first late-afternoon calibration might be avoided. For the smallest configurations we expect that the troposphere will not be a limitation on achieving the proposed goal of $100\mu$m relative positioning on all baselines. For larger configurations we estimate that while most baselines will achieve the target accuracy those baselines to recently moved antennas will have much larger errors. Further work is required to understand the effects of this on imaging and astrometry.

# 1  Introduction

An obvious requirement in an interferometer is excellent knowledge of the antenna positions. Since we need to determine antenna positions to a small fraction of a wavelength the antenna position determination is particularly acute for high frequency (sub)millimeter arrays. Wright 2002 (Memo 427) has discussed procedures for antenna position calibration as practiced at existing mm interferometers (mainly BIMA). ALMA will be a more challenging instrument on which to determine antenna positions. Although the atmosphere is superior to other mm-interferometer sites the baselines and observing frequencies are both much larger. In addition it is planned that ALMA will be operated in a unique way, as a continuously evolving 'zoom' array in which 4 antennas are moved every 2.5 to 3 days on average. The antenna location problem has to be investigated in detail to determine exactly how the array will be operated.

The present specification (Holdaway et al 2001) is that errors in antenna positions should result in uncertainties of $< 100\mu$m per baseline, corresponding to $71\mu$m per antenna if these errors are uncorrelated. This memo investigates methods to achieve this accuracy; the conclusions of this memo will be incorporated in the draft ALMA Calibration plan (Butler et al 2004). To calibrate antenna position 'geodetic VLBI' style observations will be made, rapidly cycling around a group of compact calibrators spread over the sky to measure phase and delay. It can be shown that this is the right strategy to maximise signal to noise on the position determination; roughly speaking the signal in the measured phase/delay due to an inaccurate antenna position increases linearly with angular separation on the sky (until very large separation angles) but the effect of atmospheric phase errors scale less than linearly, hence calibrator observations wide apart in angle are optimum. When the calibration observations are made both the moved antennas and some number of 'unmoved' antennas from the main array will be used. The unmoved antennas must be used so that the positions of the moved antennas can be determined relative to the rest of the array.

The questions we would like to answer are 1) Can the specified antenna position accuracy be achieved? 2) How long will the calibration process take? 3) How many 'unmoved' antennas must be included? 4) From which part of the array should the reference or unmoved antennas be taken? 5) At what time of day should the calibration observation be made? 6) What frequency should be used? 7) As noted by Wright (2002) the incremental calibration of antennas positions will cause errors to propagate. Occasionally therefore it will be useful to do a joint calibration using all antennas in the array. How often should such 'full calibration' be done?

The questions posed are quite complex and given the range of configurations sizes (with maximum baselines from 150m to 19km) it will not be too surprising if the answers to the above questions depend on the configuration. In this memo we discuss observational methods and analyse the impact of tropospheric phase errors on position determination and give estimates of the positional accuracies that can be achieved. It is aimed that a future memo will model in more detail the exact propagation of errors as reconfiguration of a zoom array proceeds.

It is clear that the following 'styles' of baseline calibration exist

(1) A 'full' calibration of the whole array using all available antennas.

(2) When moving out, antennas are taken from the array centre and placed on unoccu-

pied pads on the edge of the occupied pad distribution. In this case we could calibrate the moved antennas against one or more antennas at the array centre. One advantage of using unmoved antennas at the array centre is that it is a very long time since they were moved, and hence they will have accurate positions having been involved in many calibrations of type 1. The other advantage is that in principle only one unmoved antenna need be used. The main disadvantage of this methods is that the baselines used for calibration are long.

(3) When moving out, calibrate each of the moved antennas against the *nearest* 'unmoved' antenna. The advantage is short baselines. The main disadvantage is one unmoved antenna is needed for every moved antenna (although possibly two of the moved antenna can share one calibration antenna). Another disadvantage is that a nearby antenna may not yet have been calibrated by method-1, only method-3, and so errors will rapidly accumulate. If we restrict ourselves to unmoved antennas that have been calibrated by method-1, then as the reconfiguration proceeds the baselines used for calibration get longer, until a method-1 is inserted and again very short baselines can be used.

(4) When moving in, antennas are taken from the edge of the occupied pads and moved in to fill unoccupied pads at the centre. In this case we could calibrate the moved antennas against one or more unmoved antennas at the array outer edge. This is an analogue of method 2 adapted for inward reconfiguration, the advantages and disadvantages are similar to method-2.

(5) When moving in, calibrate each of the moved antennas against the *nearest* 'unmoved' antenna close to the array centre. This is an analogue of method 3 adapted for inward reconfiguration, the advantages and disadvantages are similar to method-3.

A good estimate of the efficiency of methods 2,3,4,5 can be made by considering single baseline calibration. In the case of methods 3 and 5 to every moved antenna there will be one baseline to an unmoved calibrator antenna which is much shorter than the rest and will dominate the solutions. In the case of methods 2 and 4, if more than one unmoved antenna is used the baselines between the moved and unmoved antennas will be much longer than the distances between the unmoved antennas. Since atmospheric phase errors will dominate over thermal noise it isected that the resulting position determination will be similar to a single baseline calibration to a single unmoved antenna.

In Sect 2 we discuss general issues of phase and delay accuracy, resolving turn ambiguities and the optimum observing frequency for calibration observations. In Sect 3 we give the theory of single baseline calibration using one moved and one unmoved antenna. In Sect 4 we extend this analysis to 'full array' calibration. In Sect 5 we discuss the required geometrical parameters that must be solved for and any constraints from the antenna location problem on instrument stability or calibration. In Sect 6 we summarise what is known about the the atmospheric parameters at the Chajnantor site. Sect 7 presents estimates of the expected antenna location accuracy for single baseline and full-array calibration. Finally in Section 8 we draw conclusions.

# 2 Using delay and phase observations

The objective of geodetic calibration observations is to measure the residual RF delay on a baseline ($\Delta\tau$, which is the total delay minus correlator model) to a number of different calibrators. These measured delays include effects of geometry and instrumental delays in different combinations toward the different calibrator. From this data set we can then solve jointly for both the antenna based geometry parameters and the instrumental effects. We can try to estimate the delay by measuring either the phase gradient across the bandpass or by measuring the observed phase (see Fig 1). The former has low signal to noise, the latter is more accurate but contains turn ambiguities and can only be measured modulo $2\pi$ (see Fig 1). These turn ambiguities arise when delay path contributions from unknown antenna positions or the atmosphere are greater than $\lambda/2$. This means that if mechanical limits on setting an antenna were $< 1$mm and if we are in the smaller configurations so that atmospheric paths were small then at 90GHz we could ignore the problem of turn ambiguities. In the general case however this is not true. Fortunately turn ambiguities can be removed by combining observations of bandpass phase gradients and phase. The former are used to resolve turn ambiguities, while the latter provide the final accurate estimate. In this scheme the bandpass delay estimate need only be accurate enough that the correct integer number of turns can be estimated.

We can express the observed phase at frequency $\nu$ on baseline 2-1 as $\phi_{obs} = \phi_{obs-unwrap}(\nu)$, modulo $2\pi$ where $\phi_{obs-unwrap}(\nu) = \phi_{delay}(\nu) + \phi_{bp2}(\nu) - \phi_{bp1}(\nu) + N$. In this expression the phase associated with RF delay on baseline 2-1 (which we call the phase-delay) is $\phi_{delay} = 2\pi\nu\Delta\tau_{21}$. The $\phi_{bp2}(\nu)$ and $\phi_{bp1}(\nu)$ terms include all the frequency dependent contributions which cannot be factorised as proportional to $\nu$. These 'bandpass' phase contributions include all phases introduced by the electronics of the bandpass and also the effect of any delay like terms introduced at IF frequencies. The $N$ term is from thermal noise. In order to reliably use the observed phase gradient across the band to resolve turn ambiguities the effect of the bandpass induced phase must first be removed (see Figure 1).

Bacmann and Guilloteau 2004 (memo in prep) have investigated how well bandpass phase can be calibrated and estimate 1° accuracies, which as we see below is sufficient to resolve turn ambiguities. They assumed however that any antenna position induced phase gradient was first removed, hence it appears that we have a problem since good antenna positions are required to get a good bandpass calibration and vice-versa. As we see below however if the non-delay like component of bandpass phase changes relatively slowly with time and is regularly monitored there should in practice be no problem.

Consider starting from completely uncalibrated bandpass phases and antenna positions. Bandpass delays (phase gradients cross bandpass) cannot be used to resolve turn ambiguities but we can instead use the phase versus time over a long observation at a single frequency in the band to resolve ambiguities. There are various ways to do this. Phases can be connected to 'unwrap' turn discontinuities and then antenna position Cartesian offsets and other quantities directly fitted. Alternatively we can first take the derivative of phase w.r.t. time to form rates, which do not have turn ambiguities and then fit these. Forming rates also eliminates the effects of time constant instrumental phase offsets. Drifts in instrumental phase do effect the rates but these in turn can can be eliminated by differencing rates between different calibrators. Using long observations of up to 6hrs or so it should be possible to derive the antenna positions
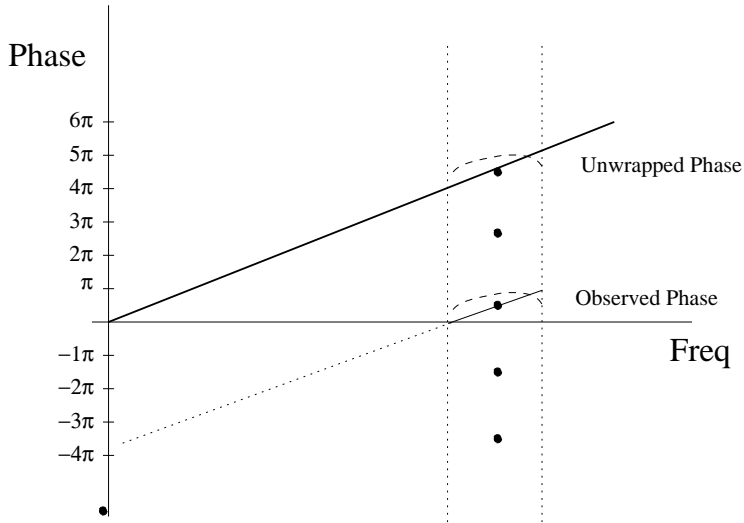
Figure 1: Illustration of observed delay and phase and how phase gradients over the bandpass can be used to remove turn ambiguities. The solid line shows the affect on phase versus frequency due to an RF delay. The dotted parallel vertical lines indicate the lower and upper range of the bandpass. The observed phase is modulo $2\pi$ and the black dots show possible values of delay phase at the band centre, all of which give the same observed phase, which is indicated by the dot in the range $-\pi$ to $+\pi$. The dashed curves indicate the effects of adding bandpass phases and IF delay effects. If this bandpass contribution can be removed the extrapolation of observed phase to zero frequency, (shown by the diagonal dotted line) can be used to resolve turn ambiguities, and so recover the unwrapped delay phase and hence the RF delay.

and other geometrical parameters. On comparing the model phase for these offsets with the observed phase the time constant antenna based instrumental phase offset at this frequency can be found. This procedure can be repeated at each frequency to derive the phase of the antenna bandpass functions. In this way it is possible to simultaneously solve for antenna positions and bandpass phase. Provided the bandpass phase varies slowly then future calibrations can use the assumed bandpass phase versus frequency to resolve turn ambiguities, first removing the bandpass phase before fitting a phase gradient. This will mean that only short observations need be used for position calibration. Also provided the original bandpasses were good enough to resolve ambiguities then the same observations can be used to incrementally update the estimates of the antenna phase bandpass functions.

What are the requirements on the sensitivity and bandpass stability to use bandpass phase gradients to resolve turn ambiguities? Turn resolution requires that the error on the bandpass group delay must be $< \lambda/2c$, corresponding to a path of $< \lambda/2$ Using bright sources it seems that sensitivity should not be a problem in meeting this goal. For a 1 minute integration on a single baseline at 90GHz the noise is $\sigma = 2.8$mJy, assuming a source of brightness S=1Jy and a bandwidth $\Delta\nu = 8$GHz, the thermal noise induced uncertainly on the group delay, expressed as a path length, is $\sigma_{\tau_{grad}} = \sqrt{12}\sigma c/(2\pi\Delta\nu S)$, which for the above parameters is $\sigma_\tau = 56\mu$m, which is much less than $\lambda/2$,

The more critical requirement to allow the resolution of turn ambiguities is on the

| Frequency (GHz) | Maximum error on bandpass phase across 8GHz to allow turn ambiguity resolution | Baseline Phase signal due to a $100\mu$m relative antenna position offset |
|:---:|:---:|:---:|
| 90 | 8° | 10.8° |
| 140 | 5° | 16.8° |
| 230 | 3.1° | 27.7° |
| 345 | 2.1° | 41° |

Table 1: Bandpass stability requirements for antenna position determination. First column gives frequency. Second column the maximum uncertainty in the phase difference across each antenna bandpass to allow phase turn retrieval. For comparison the last column gives the change in phase at each channel in the bandpass caused by a $100\mu$m position offset.

knowledge and stability of the bandpass phase. The bandpass determination/stability requirement can be expressed in terms of the uncertainty on the bandpass induced phase change across the $\Delta\nu = 8$GHz band. If this difference on the baseline is less than $180°(\Delta\nu/\nu)$ then turn ambiguities can be resolved. For the antenna specification we specify half of this value as the maximum allowed value. This antenna gradient limit is listed for various bands in Table 1, column 2. Determining the bandpass phase at these levels or better should not be a problem, since Bacmann and Guilloteau (2004) estimate accuracies of order 1°. The limitation is therefore set by the bandpass phase stability over the period between calibration observations (3 days). Note from Table 1 that the bandpass phase gradient requirements for resolving turn ambiguities get more stringent with frequency. On the other hand the mean phase change across the whole band due to a $100\mu$m position offset increases with frequency. Despite this, after considering the effects of resolving turn ambiguities and fact that we want to do the calibration under a wide range of weather conditions then 90GHz seems like an optimum frequency. Although the phase signal due to a position offset is minimised at this low frequency it is still significant when we consider the high SNR of the observations (i.e. thermal noise gives a phase uncertainty of 0.4° using 1Jy sources observed for 1 minute).

Assuming the above requirements are met then the following procedure can be followed to create an observed delay estimate for further analysis. For each observation on the baseline between antennas 1 and 2 toward a calibrator we first remove the effects of our best estimate of the bandpass phase function for each antenna $\phi'_{bp1}(\nu)$ and $\phi'_{bp1}(\nu)$. The number of phase turns is then estimated from the gradient of phase versus frequency; rounding to the nearest integer the quantity $(\nu/2\pi)(d\phi/d\nu)$, to give $N_{turn}$. The estimated unwrapped delay phase at each frequency within the bandpass can then be estimated from $\phi'_{delay}(\nu) = \phi_{obs}(\nu) - \phi'_{bp1}(\nu) + \phi'_{bp2}(\nu) + 2\pi N_{turn}$. The best estimate of the phase delay at the band centre ($\phi'(\nu_o)$) is then found by averaging over frequency. Finally we obtain the 'observed delay' for the baseline 2-1 observation, namely $\Delta\tau_{21} = \phi'_{delay}(\nu_o)/(2\pi\nu_o)$. This $\Delta\tau_{21}$ is the raw observable used in the following sections when considering how antenna positions are determined.

The observed delay depends on the antenna geometrical parameters, azimuth and elevation of the calibrator source and instrumental offsets. The instrumental offsets include the effects of tue RF delays and uncertainties in bandpass phase. Note that any

differences between the true (i.e. $\phi_{bp1}$) and assumed bandpass phase (i.e. $\phi'_{bp1}$) in their first and higher derivatives w.r.t frequency have no effect on the observed delay. Differences in the mean bandpass phase will effect the estimated delay; however this bias will be the same for all calibrators and so will give a constant offset which will be absorbed into the instrumental delay. As described in sections 5 and 7 such instrumental delay effects will be solved for and their effects eliminated as part of the antenna position estimation process. It follows that although there are constraints on the stability of the phase difference across the bandpasses (for resolving turn ambiguities) there are no such long term constraints on the stability of the mean phase averaged across the bandpass.

A final question is what are the limits on the antenna position accuracies required before the geodetic calibration can begin? A typical calibrator observation lasts say 30-60 seconds with the observations being done in spectral line mode. The bandpass group delay is estimated by Fourier transforming the phase versus frequency channel data (after removing the bandpass contribution). One limit on initial position is set by loss of coherence over the observation time. To produce a 1 radian phase change over 1 minute positions would need to be in error by over 100 wavelengths, which corresponds to 30cm is the observing frequency is 90GHz. If the a priori position uncertainty were very large then would also have to search over a large range in delay; thus requiring a high SNR to ensure that a false noise point were not identified as the real fringe. This however is not a strong constraint given the high SNR of our observations and the size of the spanned bandwidth. Assuming a total spanned bandwidth of 8GHz the width of the delay response function corresponds to a position range of 3.6cm. For a priori positions of say 1cm, we can therefore assume that the first peak in the delay response function corresponds to the fringe and there is no effect of having to search a wide range of delays.

# 3    Single baseline calibration

The most important effect limiting the accuracy of antenna positions will be the stochastic fluctuations in refractivity the troposphere due to poorly mixed water vapour. This pre-supposes that the correlator uses a highly accurate model which can take account of effects like Earth tides, Earth orientation parameters etc etc. In addition to the stochastic water vapour variations we can consider that the atmosphere has a time constant zenith delay, which we can divide into a hydrostatic part and a wet part. Even though time constant these contributions, if different above each antenna and not accurately modeled in the correlator, will affect the geometry solutions because of the different airmass to each calibrator. These systematic delay components will have negligible impact in small arrays because the unmodelled delays will be almost the same above each antenna; however when the array is in its largest configurations these systematic errors may be significant. The systematic hydrostatic delay can vary between antennas either because of pressure gradients across the site or because of difference in altitude between antennas of up to several hundred metres. Accurate barometers can be used to estimate the hydrostatic delay contribution to the systematic atmosphere errors and remove this effect in the correlator model. On long baselines differences in the total zenith *wet* total array between antennas (see Sect 5.4) might also contribute position errors.

In the discussion below we closely follow the work of Treuhaft and Lanyi (1987) in their classic paper where they discussed the impact of the troposphere on antenna positions in geodetic VLBI. We assume as they do that the phase fluctuations exist in a 'frozen screen' which moves over the array at some speed and direction. The screen is modeled as a 'slab' with some thickness and height. It is convenient to divide the refractivity variations within this slab into a constant value plus variations. If the constant refractivity term or slab thickness is different at two antennas and is unmodelled at the correlator a systematic delay error is introduced which depends on the airmass to the calibrator (see previous paragraph). Turning to the space variable wet refractivity variations within the slab, which are our main concern in this section, we assume uniform variance of fluctuations and isotropicty through the slab. The structure function of the variable refractivity in this screen is assumed to obey Kolmorgorov statistics, with the structure function on the mean square delay difference scaling as the 2/3 power of separation. This power law behavior cannot increase indefinitely and at some point there is an 'outer scale' beyond which the cross variance of refractvity no longer increases. The possible length and impact of this outer scale is discussed more fully in Sections 6 and 7.

In this section we consider the case that we have single baseline data. On one end of the baseline is an antenna which has recently been relocated and whose position we wish to determine. On the other end of the baseline is an antenna from the main array with well known position. To determine the relative position of the moved antenna interferometric observations are made in 'geodetic' style, rapidly cycling over a number of bright sources well separated in azimuth and elevation. We wish to estimate the size of the errors introduced by the wet troposphere into estimates of the relative position (and other geometrical parameters) of the moved antenna.

We consider that each individual source observation on the baseline measures one residual delay and phase (relative to the correlator model). As described in Section 2 an accurate residual delay to each source on a baseline can be obtained by first finding a low SNR estimate of the delay from the phase gradient across the band and using this to resolve the number of turn ambiguities $N_{turn}$ in the phase.

We consider that in the calibration observations we execute $N_{cycle}$ cycles (j=1,$N_{cycle}$), each cycle consisting of observations of $N_{cal}$ calibrator sources (i=1,$N_{cal}$). The data set therefore consists of $N_{cycle}N_{cal}$ measured delays. Each of the measured baseline delays between antenna 1 (the antenna with well determined position) and antenna 2 (the moved antenna) is given by

$$\Delta\tau_{21ij} = \Delta\tau_{21i}^{G} + \Delta\tau_{21ij}^{A} + n_{21ij} \tag{1}$$

Where the first term on the right $\Delta\tau_{21i}^{G}$ is the contribution due to geometry effects on the baseline between antenna 2 and antenna 1 toward calibrator i. This 'geometry' term includes the antenna based time constant instrumental delays (see section 2). We assume that the calibration session is relatively short (say 1 hour), so we ignore that the elevation and azimuth of the target source change slightly during the observation, hence the geometrical terms depend only on the calibrator source index i not on the cycle index j. Since our goal is to estimate the accuracy of the calibration method we believe this is a minor approximation. The second term ($\Delta\tau_{21ij}^{A}$) is due to the atmosphere. The third term ($n_{21ij}$)is due to the random noise in the observations.

The geometrical baseline delay can be separated into two antenna based geometrical

errors.

$$\Delta\tau^G_{21i} = \tau^G_{2,i} - \tau^G_{1,i} \tag{2}$$

The $\tau^G_{2,i}$ and $\tau^G_{1,i}$ can be thought of elements of a vectors $\tau_{\mathbf{G2}}$ and $\tau_{\mathbf{G1}}$. These geometrical delays are related to the cartesian coordinates of antenna 2 and 1 (and other potential properties of these antennas like fixed instrumental delay and non-intersecting axis offset) by matrix equations.

$$\tau_{\mathbf{G2}} = \mathbf{Bx_2} \qquad \tau_{\mathbf{G1}} = \mathbf{Bx_1} \tag{3}$$

Here each $\tau_{\mathbf{G}}$ has $N_{cal}$ rows and one column, the vectors $\mathbf{x}$ contain the geometrical parameters for the antennas and $\mathbf{B}$ is a matrix linking the two vectors. If the only source of geometrical error are the cartesian coordinates of antenna 2 then $\mathbf{x}$ is a 3x1 vector and $\mathbf{B}$ a $N_{cal}$ by 3 matrix. The content of $\mathbf{B}$ depends on the azimuths and elevations of the set of calibrator sources. The atmospheric contribution to the measured delays can likewise be divided into two antenna based parts.

$$\Delta\tau^A_{21i,j} = \tau^A_{2,i,j} - \tau^A_{1,i,j} \tag{4}$$

In contrast to the geometrical errors, the antennas based atmospheric errors $\tau^A_{k,i,j}$ are highly time dependent and therefore depend on the cycle index, j.

Let us first consider collecting one full cycle of calibrator observations (so $j = 1$), from which we then try to estimate the geometrical parameters of the moved antenna $\mathbf{x_2}$. A least squares estimate of $\mathbf{x_2}$ called $\mathbf{x'_2}$ can be made from the vector $\mathbf{\Delta}\tau$ whose elements are $\Delta\tau_{211j}$ (see Equ 1) via

$$\mathbf{x'_2} = \mathbf{F}\mathbf{\Delta}\tau \tag{5}$$

where

$$\mathbf{F} = (\mathbf{B'B})^{-1}\mathbf{B'} \tag{6}$$

More generally account can be taken of the different atmospheric random errors contributing to the $\tau$ elements by taking a weighted least squares solution where

$$\mathbf{F} = (\mathbf{B'W'WB})^{-1}(\mathbf{B'W'W}) \tag{7}$$

where weight $\mathbf{W}$ is a matrix whose diagonal elements are proportional to one over the variance of the measurements, and whose off-diagonal elements depend on the expected cross-correlation of the atmospheric errors.

Least-squares methods simply find the best set of antenna parameters which give predicted measurement which are as close as possible to the actual measurements in a least-squares sense. Strictly speaking instead what we wish to minimise is the least squares difference between the estimated and true *antenna parameters*. This can be done using Wiener filtering methods if we know the statistical properties of the expected antenna parameters and the atmospheric phase errors. An optimum matrix $\mathbf{F}$ based on such Wiener filtering can then be devised. This is especially useful if there are parameters like antenna axis offsets which we might wish to solve for but at the same time wish to take account of their small expected variance. In geodetic VLBI more sophisticated Kalman filtering methods are used, where the variance on the

solutions are used recursively to optimise covariance matrices which then in turn alter the inversion matrix $\mathbf{F}$. For the relatively short runs of data we are expecting for ALMA position calibration it is unclear whether such methods will be significantly better than others. In this memo we assume the simple unweighted least squares estimate for $\mathbf{F}$ given in Equ 6.

Whatever the form of $\mathbf{F}$ we can write that

$$\mathbf{x_2'} = \mathbf{F}\Delta\tau = \mathbf{x_2} - \mathbf{x_1} + \epsilon \tag{8}$$

So the estimate of cartesian coordinates for antenna 2 are equal to the actual cartesian coordinates for antenna 2 plus any position errors antenna 1 had, plus the $\epsilon$ term which depends on the atmosphere and thermal noise

$$\epsilon = \mathbf{F}(\tau_2^\mathbf{A} - \tau_1^\mathbf{A}) + \mathbf{Fn} \tag{9}$$

Where the elements of the vector $\tau_2^\mathbf{A}$ are formed from the atmospheric delays to each of the calibrators from antenna 2 within the cycle, likewise for $\tau_1^\mathbf{A}$ from antenna 1. We assume from now on that our observations are high SNR so that the noise term can be neglected.

We can generalise to analysing $N_{cycle}$ cycles of calibrator observations, by noting that we can apply the above analysis for each cycle to obtain an $\mathbf{x_2'}$ estimate and then average the results. The resulting error vector is

$$\epsilon = \frac{1}{N_{cycle}} \sum_j \mathbf{F}(\tau_\mathbf{2j}^\mathbf{A} - \tau_\mathbf{1j}^\mathbf{A}) \tag{10}$$

where $\tau_\mathbf{2j}^\mathbf{A}$ and $\tau_\mathbf{1j}^\mathbf{A}$ are vectors of baseline atmospheric errors to different calibrators for cycle $j$ and antennas 2 and 1. Converting from vector notation we find that the l'th component on the error vector for the position of the moved antenna 2 is

$$\epsilon_l = \frac{1}{N_{cycle}} \sum_j \sum_i F_{li}(\tau_{2,i,j}^A - \tau_{1,i,j}^A) \tag{11}$$

We can now consider the statistical properties of the components of the estimate error, including variance and covariance. Using the above equation the ensemble average of the product $\epsilon_l \epsilon_{l'}$ is

$$\langle \epsilon_l \epsilon_{l'} \rangle = \frac{1}{N_{cycle}^2} \sum_i \sum_{i'} F_{l,i} F_{l',i'} \sum_j \sum_{j'} \left\langle \tau_{2,i,j}^A \tau_{2,i',j'}^A \right\rangle - \left\langle \tau_{2,i,j}^A \tau_{1,i',j'}^A \right\rangle - \left\langle \tau_{1,i,j}^A \tau_{2,i',j'}^A \right\rangle + \left\langle \tau_{1,i,j}^A \tau_{1,i',j'}^A \right\rangle \tag{12}$$

In the general case (especially of short baselines) it is important to take into account the vertical structure of the atmosphere. We can divide the atmosphere into layers so that

$$\tau_{k,i,j}^A = \sum_m \tau_{k,i,j,m}^A = \sum \frac{\Delta z}{\sin(\theta_i)} \chi_{k,i,j,m} \tag{13}$$

where $\Delta z$ is the layer thickness, $\theta_i$ the zenith angle of observations to source i, and $\chi_{k,i,j,m}$ the refractive index at layer m, along the ray to a source i in cycle j, from

antenna k. Substituting Equ 13 in Equ 12 and using the following expression for the structure function (Treuhaft and Lanyi 1987)

$$D_\chi(\mathbf{\Delta r}) = 2\langle \chi^2 \rangle - 2\langle \chi(\mathbf{r_1})\chi(\mathbf{r_2}) \rangle \tag{14}$$

we obtain

$$\langle \epsilon_l \epsilon_{l'} \rangle = \frac{\Delta z^2}{2N_{cycle}^2} \sum_i \sum_{i'} \frac{1}{\sin(\theta_i)} \frac{1}{\sin(\theta_{i'})} F_{l,i} F_{l',i'} M_{i,i'} \tag{15}$$

where

$$M_{i,i'} = \sum_j \sum_{j'} \sum_m \sum_{m'} D_{\chi,2,i,j,m,1,i',j',m'} + D_{\chi,1,i,j,m,2,i',j',m'} - D_{\chi,1,i,j,m,1,i',j',m'} - D_{\chi,2,i,j,m,2,i',j',m'} \tag{16}$$

Where we have assumed that $\langle \chi^2 \rangle$ is the same above each antenna. In this expression $D_{\chi,k,i,j,m,k',i',j',m'}$ is the structure function (mean cross correlation about the mean) of refractivity between two points in the moving phase screen denoted by indices $k, i, j, m$, and $k', i', j', m'$ (corresponding to two sets of indices for antenna, calibrator source, cycle number and layer number). The isotropic, uniform, frozen screen model assumes that $D_\chi$ is a function only of $R = |\mathbf{\Delta r_{k,i,j,m,k',i',j',m'}}|$ the length of the vector between the two points within the moving screen. Note that in Equ 16 $D_{\chi,2,i,j,m,2,i',j',m'} = D_{\chi,1,i,j,m,1,i',j',m'}$ but that for the general case when the wind direction is not perpendicular to the baseline $D_{\chi,1,i,j,m,2,i',j',m'} \neq D_{\chi,2,i,j,m,1,i',j',m'}$.

In the normal assumption of Kolmorgorov turbulence we have that

$$D_{\chi,k,i,j,m,k',i',j',m'} \propto R^{2/3} \tag{17}$$

At some outer scale L we reach the scale at which energy is introduced into the system (which then cascades to smaller scales according to the Kolmogorov theory)- beyond these scales the variations in refractive index will saturate. To take into account of this effect Treuhaft and Lanyi (1987) proposed a modified law which is

$$D_{\chi,k,i,j,m,k',i',j',m'} \propto R^{2/3}/(1 + (R/L)^{2/3}) = f(R) \tag{18}$$

More discussion about the outer scale and its meaning in the context of ALMA is given in Section 3.

We are mainly interested in the variances on the antenna geometrical parameters, i.e. when $l = l'$. A convenient way to visualise how the variance is calculated from equations 15 and 16 is to think of all the control points where a ray from an antenna cuts a layer in the phase screen. Each point is characterised by indices k,i,j,m, for antenna k, calibrator j, cycle k and layer m. For estimating the variance on parameter l, we each point having an associate a weight given by

$$w_{l,k,i,j,m} = \frac{(-1)^k F_{l,i}}{\sin \theta_i} \tag{19}$$

then consider all the possible pairs of control points and their separations in space R. Each pair contributes to the variance estimate on parameter l, i.e. $\langle \epsilon_l \epsilon_{l'} \rangle$ a term proportional to $w_{l,k,i,j,m} w_{l,k',i',j',m'} f(R)$.

11

In their paper Treuhaft and Lanyi (1987) used similar expressions to derive the structure function of the observed delay on a baseline as a function of baseline length $b$ while observing a source at some elevation $\theta$, namely $D_{\tau,\theta}(b)$. They found that $D_{\tau,\theta}(b) \propto b^{5/3}$ for $b < t$ where $t$ is the layer thickness while $D_{\tau,\theta}(b) \propto b^{2/3}$ for $b > t$. It is important to understand that this change in observed power law is not due to reaching the outer scale of $D_\chi$ but is simply due to the thickness of the layer. For still longer baselines it is possible to get an even shallower power law approaching 0 when $b$ exceeds $L$ (see VLA results reported by Carilli and Holdaway 1999 (Memo 262)).

# 4    Multi-antenna position calibration

In the previous section we considered the errors introduced by the stochastic atmosphere into antenna positions when 'single baseline' calibration is carried out. Here we generalise to the case of multiple antennas involved in the calibration and the resulting atmospheric errors that are introduced into antenna relative positions. A special case of multiple antenna calibration is when all available antennas are used in the calibration (the case of 'full array calibration' as defined in Section 1).

In Sect 4.1 we discuss the statistics of the position errors for a single 'full' calibration calibration run. The results describe the final antenna errors that would result if all antennas had undetermined positions and we are attempting to solve for these positions. The solution presented applies directly to the problem of solving for antenna positions when we are 'stopped' in the smallest or largest array of ALMA (see Section 8).

For intermediate baselines because of continuous reconfiguration all antennas will not have equal a priori position errors. Instead four recently moved antennas will have large position errors while the remaining antennas, which have had the opportunity to be involved in many calibration runs, will have much better positions. A full calibration of all antennas provides a new estimate of their relative positions. In section 4.2 we consider how to combine this solution with existing information to provide the best estimate of the array geometry. Finally in Sect 4.3 we discuss the possibility of directly imaging the atmospheric phase screen using data from antennas with good positions and using this information in the antenna position solutions.

## 4.1    Relative antenna position accuracy obtained from a single full-calibration

Here we consider the achievable accuracy when a 'full calibration' of the whole array of N antennas (usually between 60 and 64) is carried out. If the calibrator is a point source then it is well known that the antenna based delay for a given antenna can be derived within a constant by adding up all the delays for the baselines involving this antenna and dividing by N. [Note if the calibrator is not a point source, as is possible for larger arrays, the calibrator can be imaged purely using closure quantities and then the effect of the structure phase/delay removed from all data, making it effectively a point source, as is done in VLBI imaging]. There no loss in generality in using the above method of converting baseline delays to antenna based delay quantities. The method finds a set of antenna based delays consistent with all the data. Stated mathematically the method gives an estimated antenna based error of

$$\tau'_{aij} = \frac{1}{N} \sum_{b=1, b \neq a}^{N} \Delta\tau_{baij} = \tau_{aij} - \frac{1}{N} \sum_{b=1}^{N} \tau_{bij} \tag{20}$$

where $\Delta\tau_{baij}$ is the observed delay between antennas 'b' and 'a', toward calibrator i in cycle j, and is such that $\Delta\tau_{baij} = \tau_{bij} - \tau_{aij}$, where $\tau_{aij}$ and $\tau_{bij}$ are the true antenna based delays above 'a' and 'b'. Note that the last term of the above equation forms a constant which is the same for all antennas toward calibrator i in cycle j.

Following the argument in Section 3, for a single cycle (j=1) we can form a vector $\tau'_\mathbf{a}$ whose elements are obtained from the different calibrators i from Equ 20. The best estimate vector $\mathbf{x'_a}$ of the geometrical parameters for antenna 'a', $\mathbf{x_a}$ is then obtained from

$$\mathbf{x'_a} = \mathbf{F}\tau'_\mathbf{a} = \mathbf{x_a} - \bar{\mathbf{x}} + \epsilon_\mathbf{a} \tag{21}$$

where $\bar{\mathbf{x}}$ is a vector whose elements are the average of all the antennas geometrical parameters and where $\epsilon_a$ is the error introduced by the atmosphere into the geometrical parameters for antenna 'a'.

If we estimate geometrical parameters for each cycle and then average over $N_{cycle}$ cycles then we obtain that for the l'th geometrical component for the a'th antenna

$$\epsilon_{al} = \frac{1}{N_{cycle}} \sum_j \sum_i F_{li} \left[ \tau^A_{a,i,j} - \frac{1}{N_{ant}} \sum_{b=1}^{N} \tau^A_{b,i,j} \right] \tag{22}$$

the last term being independent of 'a' and hence the same for all antennas. For interferometry all that is relevant is the difference in position errors between antennas. The relative difference in geometrical component l between antennas 'a' and 'b' is given by

$$\Delta\epsilon_{abl} = \epsilon_{al} - \epsilon_{bl} = \frac{1}{N_{cycle}} \sum_j \sum_i F_{li} (\tau^A_{a,i,j} - \tau^A_{b,i,j}) \tag{23}$$

This has exactly the form of Equ 11 obtained for the single baseline case. Hence for 'full array' calibration we can estimate the variance of geometrical component l for $\Delta\epsilon_{abl}$ for antennas a,b f by substituting $l = l'$ in Equ 15,16 and using the structure functions above antenna a and b instead of 1 and 2.

The similarity in the expected errors for single baseline and 'full array' calibration is perhaps an unexpected result, it might have been thought intuitively that with many more antennas involved a smaller rms error would have been expected. The result shows that if we do single baseline calibration say between an antenna at the centre of the array (antenna 1) and one at the edge (antenna 2) then we obtain a certain rms error on the Cartesian coordinates of the separation, given by Equ 15 in Sect 3. If we instead perform a full-array calibration using all antennas, for the same observing time, and using the same calibrator pattern, then the rms error on the Cartesian coordinates of the separation between antennas 1 and 2 is the same (note this assumes thermal noise and other baseline based noise sources are negligible compared to antenna based atmospheric errors).

Given the above it might be wondered whether there is any advantage in doing full array calibration over single baseline calibration. In fact there is an advantage. Consider the example in the previous paragraph from the point of view of an antenna

3 which is located close to antenna 2. After doing full array calibration the rms in the position difference between antenna 2 and 3 depends on the distance between antenna 2 and 3 and so is relatively small. In contrast after doing single baseline calibration of antenna 2 using antenna 1 then antenna 2 has a large rms error because of the large antenna 1 to 2 distance. This error translates directly into a large antenna 2 to 3 error. The point is that the full array calibration gives large errors across the array, but these errors are correlated on small scales, leading to small errors on short baselines. In contrast in single baseline calibration of an antenna 2 at the edge of the array using antenna 1 at the centre there are no such correlated and compensating shifts for the position of antenna 3.

## 4.2  Optimum antenna position estimation for continuous reconfiguration

The analysis presented in Sect 4.1 shows the errors on antenna relative position error from analysing a single calibration run. If this were our only information, as would be the case if all antennas started with completely uncalibrated positions, the resulting statistics would represent our best estimate of antenna positions. Instead the normal situation with ALMA in its intermediate configurations is that a subset of 4 recently moved antennas will have much worse positions while the rest of the antennas. In this case the new information from a single noisy calibration run giving the relative antenna separation must be combined optimally with existing a priori information.

One way to approach to the problem, which is followed in geodetic VLBI, is to do a global solution of all pad positions simultaneously fitting data from all calibration runs. It is difficult to theoretically calculate the resulting statistics for an continuously reconfiguring array. Estimates can however be made by a Monte-Carlo simulation where realistic measurement baseline delays to the calibrators are generated for each of $N_{conf}$ configurations. These can be factorised by antenna according to Equ 20, producing a very large vector which is of length $N_{conf}N_{cycle}N_{cal}N_{ant}$. The state vector to be estimated, $\mathbf{x}$, contains all the pad positions and other antenna based errors plus terms to account, in each configuration, for a common offset of all pads in x,y,z. The two vectors are linked by a very large matrix $\mathbf{B}$. To get a optimum solution a weighted least squares (see Section 3) solution incorporating the expected variance and covariances on the measurements should be used.

Another way to look at the problem is in terms of Bayesian statistics, where new information (from a new cal run) is added to old data (the a priori positions of the pads). A parallel (and possibly equivalent approach?) is to view the problem in terms of Wiener and Kalman filters (see Section 3). The Wiener filter can incorporate a priori estimates to create a new estimate if the covariance matrices of both the data errors and of priori position errors are inputted. The data covariance matrix can be estimated from our atmospheric model, and that of the a priori positions initially guessed. The Kalman filter is a generalisation which generates an updated a priori position covariance matrix based on the quality of the fit for each configuration, which then can be used in the fitting for subsequent configurations.

More work is needed to simulate the position errors in a continuously reconfiguring array and these can hopefully be presented as part of a future memo.

## 4.3 Turbulent screen imaging

Another approach to the antenna position optimisation problem would be to use delay measurements from antennas with well calibrated positions towards multiple calibrators to directly image the structure of the turbulent phase screen. For smaller configurations with typical antenna separations comparable to the thickness of the turbulent layer such imaging should be 3D and tomographic. For larger configurations only a 2D screen need be estimated. Assuming the 'frozen-screen' assumption, and determining the screen velocity the screen model could then be used to remove atmospheric phase errors above antennas whose positions we wish to determine, before being solved for in the normal way (see Section 3).

The accuracy of such a screen imaging method may depend on whether the array is expanding or contracting in size. If the array is contracting the newly occupied pads will be at the centre and surrounded by well positioned antennas and the method should work well. In the case of array expansion however the newly occupied pads will be at the perimeter. In this later case the efficiency of the method will also depend on the orientation of the screen velocity vector compared to the vector from the pad to the centre of the array. If these two vectors are nearly parallel then the same portion of the phase screen which affects a pad will just before or just after pass over the bulk of the array. In this case relatively good delay correction should be achieved. In contrast if the two vectors are close to orthogonal the correction will be significantly worse.

# 5 Required geometrical and instrumental parameters

Whether we do single baseline calibration (see Section 3) or multiple antenna calibration (see Section 4) the final accuracy will obviously depend on the number and size of the antenna geometrical parameters that must be solved for. Here we discuss which of these potential antenna based quantities are likely to be significant.

Explicitly Equ 3 shows that the geometrical contribution to the delay at an antenna toward a particular calibrator is represented by a matrix $\mathbf{B}$ multiplying a vector $\mathbf{x}$ which contains the geometrical parameters of an antenna (essentially the same equation holds in multiple antenna calibration, See Sect 4.1). In the simplest possible case only three components, the antenna Cartesian coordinates are needed. In this case the elements of $\mathbf{B}$ linking the calibrator delays to these Cartesian coordinates depend on the sines and cosines of the calibrators elevations and azimuths. More generally other instrumental and geometrical terms can effect the delay, these include instrumental delays, non-intersecting axes effects and zenith delays due to the dry or wet atmosphere. We need to consider the potential contribution of each effect on the data (taking into account possible ancillary calibration) and then whether this parameter should be estimated from the astronomical observations.

## 5.1 Time constant Instrumental Delays

Delays introduced by the electronics and propagation through the antenna optics will be a minimum necessary extra quantity to estimate. This makes the fourth column of $\mathbf{B}$ in Equ 1 all ones. One can visualize dealing with time constant delays by differencing the

observed delays between all calibrators and a reference calibrator, and then fitting these difference delays. Alternatively one can think of fitting explicitly for the instrumental delay at each antenna using a solution matrix **F** incorporating the inverse of matrix **B**. The solution in both cases will be the same.

As explained in Section 7 whether or not one needs to solve for a time constant delay or not has a surprisingly significant affect on the accuracy of the z -coordinate estimate. For this reason in geodetic VLBI the instrumental delay is continuously measured. A 'comb' of tones is injected at the front end and their phase detected further down the data path, either at correlation or at the antenna prior to digitisation. From the phase gradient across these detected tones the instrumental delay is measured. There are no plans for such a device for ALMA.

## 5.2 Time variable instrumental delays

It is important to consider whether it is necessary to also solve for the first or higher derivatives of instrumental phase versus time. The current draft of the ALMA system technical requirements (Sramek 2004) specifies that over 300sec the maximum change in delay due to the electronics is 22 fsec, corresponding to $6.6\mu$m of path change. The specification was derived to be smaller than the stochastic changes due to the atmosphere over the same interval in the best (i.e. 95% percentile) conditions. There is also the specification that variation in the antenna structure causes less than 13 fsec changes, or $4\mu$m. This latter specification only applies to changes in antenna position on the sky of less than 2 degrees; there is no specification for the change over very large angles as required for antenna position calibration, hopefully however these should still be much smaller than the required antenna position error.

A potential concern with the instrumental phase drift specification for antenna position calibration is that it allows systematic drifts in phase, which can accumulate to give large phase differences over the 30-60 minutes or so it takes to do a full antenna position calibration. A simple way to minimise the effect of linear instrumental phase drifts on antenna position determination is to have a cycle pattern consisting of two half-cycles where the calibrators are observed in the opposite order. Such a cycle also has the practical advantage that cable wraps are avoided. Following Section 3, the analysis of multiple half cycles, can be considered as solving for the antenna geometrical parameter from each half-cycle of data and averaging the results (see Equ 10). Since the matrix operation is a linear operation, any time linear instrumental delay added to the antenna based $\tau$ in Equ 10 will give equal and opposite errors in each half cycle and hence will cancel out. The only approximation involved in this is that because of source movement across the sky the **F** matrix in Equ 10 are not exactly the same from half cycle to the next, but the difference introduced over the 5-10 minutes between one half-cycle and the next will be negligible.

With two back-to-back half cycles quadratic variations of phase versus time *will* contribute to the derived antenna positions. However given the present specification of less than $6.6\mu$m variation over 300sec it is expected that these will produce errors of less than $6.6\mu$m in antenna positions.

16

## 5.3 Axis offsets

Another potential geometric parameter to measure is the change in the 'axis offset' between the elevation to azimuth non-intersecting axes from its nominal value assumed in the correlator model. If this offset must be estimated it introduces entries into the 5th column of $\mathbf{B}$ in the i'th row of $\cos(\theta_i)$, where $\theta_i$ is the elevation of the i'th calibrator. The antenna specifications imply that in normal operation of moving antennas the non-intersecting axis will vary by less than $30\mu$m (ALMA antenna specification 2004), this is less than the target accuracy for the cartesian coordinates. This means in normal operation it will not be necessary to estimate it. This is good, since as described in Section 7 making such an estimate further increases the rms on the z coordinates. The antenna specification does however note that in the case of large shocks to the antenna, the $30\mu$m stability does not apply, it may therefore be occasionally necessary to estimate non-intersecting offsets.

## 5.4 Systematic atmosphere effects

The derivations given in Section 3 and 4 for the effects of the atmosphere concerned the stochastic effects of water vapour. We can consider these stochastic fluctuations to be superimposed on a slowly time varying zenith delay above each antenna. The part of this integrated zenith delay path which is different between two antennas and is unmodelled at the correlator ($\Delta z$) will introduce delays proportional to approximately $\Delta z/c\sin(\theta)$ which will then affect the antenna Cartesian coordinate estimates, particularly the z component.

The systematic zenith delay above each antenna can divided into a hydrostatic part which is proportional to ground pressure and a wet part which depends on the total water vapour column. The zenith delay above antennas will be different because of both horizontal gradients in zenith delay and due to difference in altitude between antenna sites. Below we discuss only the effect of horizontal gradients, altitude affects will be considered elsewhere.

Chen and Herring (1997) have discussed the effect of systematic horizontal gradients in zenith delay on VLBI geodetic measurements. In the VLBI context the effect of such gradients is to cause an azimuthal dependence in delay across the sky at uncorrelated sites. This is different from the ALMA connected element case where the atmosphere is still highly correlated and we wish to know the direct effect of horizontal delay gradients. Despite this the work done on the VLBI case can be used to estimate the amplitude of these gradients. From both observations and numerical weather models applied to (mostly) sea level VLBI sites such as Westford, MA, Chen and Herring (1987) found gradients at the zenith of rms order 0.2mm/radian. The gradients were typically correlated over periods of a few days. The rms due to pressure gradients was about a factor of two larger than the gradients due to the wet atmosphere. At the much drier ALMA site we can expect that the pressure contribution will be even more dominant. Converting to horizontal pressure gradients by assuming a dry atmosphere scale height of 5km, the VLBI results imply sea level horizontal pressure gradients giving 40mm of zenith path change over 1000km. This is consistent with typical variations in sea-level pressure of order 20mb over 1000km as seen in typical isobar weather maps (where we note that 1000mb = 2.6m of path). If as expected the horizontal gradients scale with pressure then at the ALMA site we can expect rms delays of 12mb or 30mm per

1000km). In its largest Y+ configuration ALMA has longest baselines of 19km and typical baselines of 10km, over which typically pressure gradients introduce $300\mu$m delays, which is much larger than our target antenna position accuracy.

Chen and Herring (1997) investigated the effect of using global numerical weather models to estimate and remove the effects of dry and wet horizontal delay gradients in VLBI data. This modeling appeared to reduce the rms gradient effects by a factor of 2 or 3. It is unclear how successful such an approach would be at the ALMA site; if the dominant residual error in the VLBI case was due to wet delay gradients then it may actually be more successful for ALMA because presumably the wet term will be much less significant at ALMA.

An alternative approach is to use weather monitoring devices to estimate gradients. The dry zenith delay gradient can be estimated using measurements from a distributed barometer network and corrections introduced into the correlator model or post-correlation calibration. At the time of writing the proposed ALMA barometer accuracy (defined primarily from antenna pointing) is 0.5mb (see Hills et al 2004). Such a specification does not seem to be sufficient to estimate pressure gradients across the largest configurations. More accurate bolometers are available at higher cost and we can consider using a network of bolometers with 0.1mb accuracy distributed over the site. Given that we have a limited limited number of such bolometers and do not wish to estimate second derivatives then assuming typical second order spatial derivatives for pressure are of order 20E-6 mb/km and assuming a bolometer accuracy of 0.1mb then bolometer separations of order 50km are optimum for estimating pressure gradients. Let us consider distributing say 6-7 bolometers (and other atmosphere sounding equipment) at permanent sites (i.e. associated with pads and not antennas) around the perimeter of the ALMA site and near the centre (over a diameter of 20km). The location of these weather stations should be carefully considered in order to be able to estimate both horizontal pressure gradients and the atmosphere lapse rate (needed in order to estimate pressure differences with pad altitude above sea level). Such a network would probably able to reduce zenith delay differences over 10km to less than $100\mu$m.

Finally we can also try to estimate systematic gradients in the zenith *wet* delay with measuring devices. Geodetic VLBI uses Water Vapor Radiometers to try to estimate the total zenith term, with mixed success. Unlike the WVRs used for ALMA the geodetic WVRs are optimised for long term stability. The ALMA WVRs are also mounted on the antennas, which in all but the largest configurations is not optimum for determining gradients. It might therefore be useful to also site WVRs, perhaps specially optimised for long term stability, at the fixed pad locations.

It is worth noting that either input from measuring devices or numerical models is needed not just when determining antenna positions but also during fast switching observations. For fast switching with a elevation difference between calibrator and target of 3 degrees observed at elevation of 45 degrees then on 10km baselines at 900GHz the typical uncorrected zenith delay gradients of 12mb/1000km, introduces rms $24°$ phase errors. With bolometer corrections the resulting rms phase contribution can be reduced to one third of this value. For snapshot observations the effect of zenith delay gradient phase errors is simply to shift the target source position, they do not limit imaging dynamic range. For snapshot astrometry projects several calibrators could be used to estimate and correct for the induced shift. In contrast for long tracks

even a none time varying gradient does effect image dynamic range, because each component snapshot image has its own RA,dec shift.

If there are significant variations is zenith delay between antennas which are not modeled in the **F** matrix the results for the antenna positions are biased (see Section 7). If we include estimating an independent zenith delay at each antenna the **B** matrix must have another column with $1/\sin(\theta_i)$ entries, and the effect of this can be incorporated in the corresponding **F** inversion matrix. As described in Section 7, if we must solve for a zenith delay at every antenna this greatly increases the z rms. There is an interesting difference here between single baseline calibration and 'full array calibration'. In the former case in the presence of a delay gradient we must effectively solve for an extra parameter for the moved antenna (which is the difference in zenith delay to the stationary antenna) and the number of parameters solved for significantly increases and so does the rms errors. In contrast for a full array calibration the overhead introduced by estimating a delay gradient is not large since only two extra unknowns must be solved for compared to the 4N unknowns for Cartesian coordinates and instrumental delays. In this second case it is not expected that including a delay gradient estimate will significantly increase the z rms. This suggests that if external devices are not sufficient to remove delay gradients for large configurations it is desirable for antenna position calibration to use a significant number of antennas in the calibration and perhaps the whole array.

# 6  Assumed Atmospheric Stochastic Parameters at Chajnantor

The main source of information about the phase structure of non-systematic, stochastic part of the atmosphere at the ALMA site comes from the two site test interferometers (built by NRAO and ESO respectively). There are extensive data sets from these instruments which allow the seasonal and daily variations in phase stability to be tracked. Both interferometers have baselines of 300m which allows the structure function of the atmosphere on scales less than 300m to be determined, but they provide almost no information about longer correlation scales.

Holdaway et al (1995, memo 129) analysed early results from the NRAO test interferometer. The instruments data gives a rms difference in phase for the baseline phase over different time intervals. This quantity can be related to the rms phase difference instantaneously as a function of baseline separation (i.e. $\sqrt{D_\tau(b)}$ for scales $b < 300$m). They found exponents for the power law dependence of rms phase versus b which ranged from -0.33 to -0.83. These agree well with the theory proposed by Truehaft and Lanyi (1987) which predicts exponents of 1/3 and 5/6 when $b > t$ and $b < t$ respectively. These results imply a varying thickness of the turbulent layer. The fact that the exponent was at a minimum when the total phase errors were small suggested a two phase medium with a thin ever present layer of $t < 300$m and a thicker layer of very variable strength (mainly present during the day). The thin layer was assumed to be associated with the inversion layer that forms above the site. An important parameter of the turbulent layers is their height, $h$ (note Treuhaft and Lanyi did not distinguish between layer thickness and height, the assumed the turbulence extended right down to the ground and characterised it by one parameter its thickness/total

height which they called $h$). By comparing data on the two interferometers Robson et al 2001 (memo 345) was able to estimate the height of the turbulent layer, finding that it was usually in the range 300m to 500m. Further analysis by Delgado (2001, memo 361) found that turbulent layer heights were systematically smaller at night.

An important parameter which is so far not well constrained from observations is the outer scale of the turbulence. Observationally at the site all we know is that because the smallest phase power law exponent observed with the 300m baselines is $-0.33$. the outer scale is $L > 300$m (Holdaway et al 1995). For their analysis of geodetic VLBI Treuhaft and Lanyi used an effective outer scale of 3000km(!), which was simply chosen to make the model predict mean rms fluctuations of 2.5cm in zenith path over a day at a sea-level VLBI site. In contrast observations at the VLA measured in one case an outer scale of 6km (Carrilli and Holdaway 1999, memo 262).

Theoretically the outer scale should correspond to the scale of the eddies which inject power into the system. For energy injection from convection scale sizes comparable to the layer thickness are expected, which then predicts outer scales of $\approx 1$km (Ishimuru 1997). The reason for the very discrepant estimates of outer scale given above is probably that energy is injected into the turbulence at several different scales by different physical process. Each process then has its own Kolmogorov cascade down to small scales. Convection and ground layer viscosity sources have outer scales of kilometers while weather systems have scales of 100's km. A full plot of rms phase versus baseline length would probably show a flattening in the range 1km - 100km and then an increase on longer baselines till the rms fluctuations in zenith delay over several days corresponding to 3000km approaches the observed saturation value of 2.4cm at sea-level. For the case of ALMA antenna position calibration the relevant outer scale is the first one (independent of weather systems) which we guess is in the range 1km (theory) to 6km (VLA observations). Unfortunately as we see below, in the larger configurations the achievable accuracy of the antenna position calibration is a strong function of this poorly known outer scale size; any observation which could constrain it would therefore be very welcome.

In contrast to the outer scale the diurnal and seasonal variations in atmospheric phase stability at the site are well know, as shown in Figure 2. Plotted in this figure is the rms delay fluctuations on the 300m baselines measured in microns. To maximise the usefulness of our analysis we give in the following sections the rms errors on the antenna coordinates in units of this 300m rms path fluctuation. One caution is this plot is averaged over several days and hours in each axis, and there are short term variations in the rms. Another caution is the the results are derived from a 11GHz interferometer and some of the nighttime structure is probably due to the ionosphere (Hales et al 2003, memo 459) - which will not effect significantly millimeter observations.
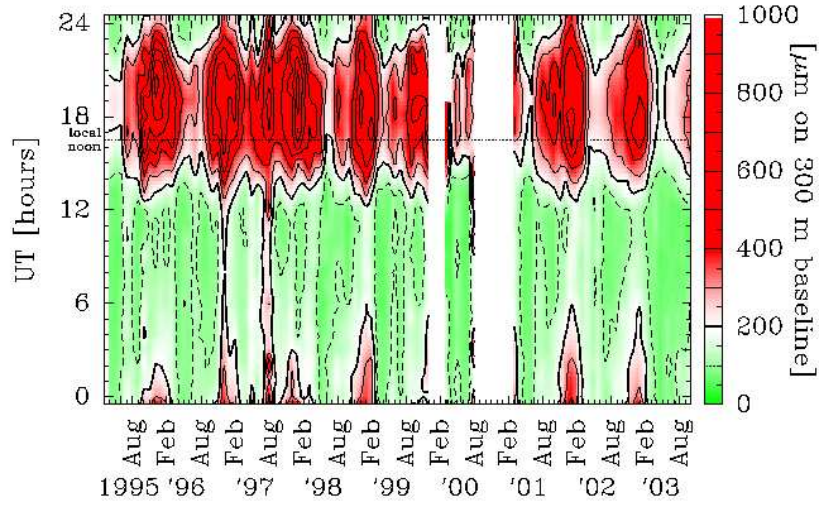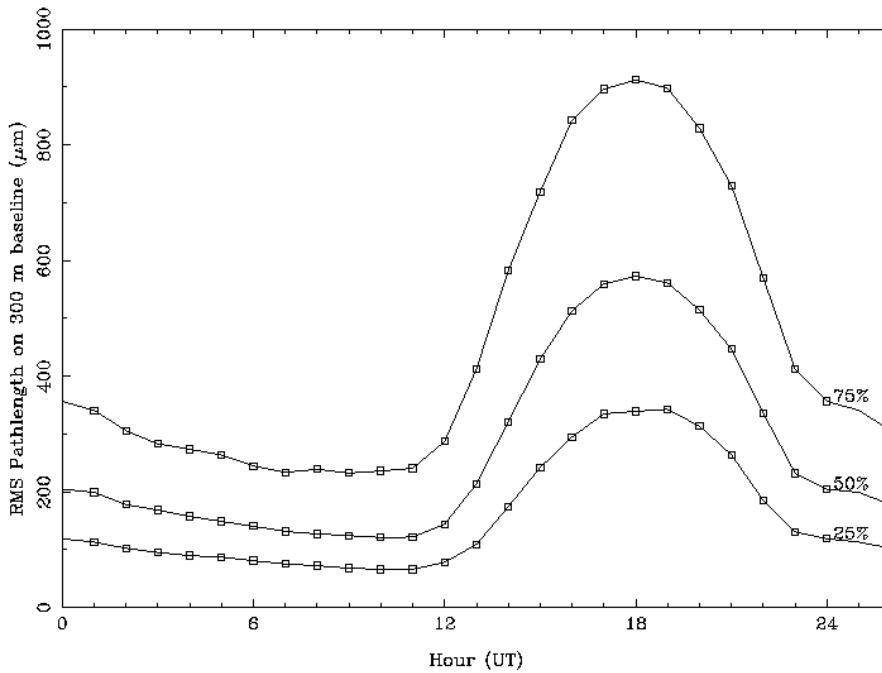
Figure 2: **Top**. RMS zenith atmospheric path length error on 300m baselines as a function of time of day and time of year. **Bottom** Seasonal averaged, diurnal variations in 300m rms atmospheric path lengths.

# 7 Calibration Simulation Results

The variance on the x,y,z coordinated of the moved antenna were estimated by evaluating equations 15 and 16 in a MATLAB code. In addition a Monte-Carlo MATLAB

program was created to create model phase screens, and then calibrate antenna positions, to check that the statistical model gave correct results. In order to investigate dependencies on baseline length and other variable the Monte-Carlo simulations were too much too slow and so in the discussion below only the results of the statistical model are presented. The Monte-carlo method did however provide a useful verification of the statistical method.

In solving for position and other parameters in the statistical code the inversion matrix $\mathbf{F}$ was calculated assuming simple least squares fitting (Equ 6). No attempt was used to use weighted fitting (see Equ 7), it is not thought this would significantly change the results. As mentioned in Section 3 other inversion methods based on Wiener or Kalman filtering can be used, these have not yet been implemented.

An input parameter to our simulations was the sky distribution of calibrators. Initially we took as our calibrator set 5 different calibrators, one at the zenith and one above the east, west, north and south horizons respectively. We later varied the exact number and orientation of the calibrators to check for any strong dependencies. In our standard run we assumed that the baseline was East-West and the wind direction was at 45° to this. We again varied the relative wind and baseline orientations to again check for strong dependences. We finally checked the effect of adding small perturbations from the geometrically perfect distribution of order 10° and found only small effects on the recovered position errors. Using the geometrically perfect distribution is therefore justified and we concentrate on this pattern since the connections between the measured delays and the derived coordinates are clearer.

An important parameter in the 5 calibrator pattern was the elevation of the four 'horizon' sources. To determine this we varied the elevation of these sources and looked at the rms errors of x,y,z. We found that the optimum elevation used depended somewhat on which parameters were being solved for. For the standard problem of solving for cartesian coordinates and a constant instrumental delay offset we found an optimum for estimating the z coordinate (which as we see is the dominant error) when the elevation was about 30°. This was a compromise between having a large difference in elevation between zenith and horizon sources to maximise the delay difference signal due to the antenna z coordinate and not having too low an elevation which then has a large atmospheric contribution.

A full calibration cycle consisted of two half cycles, passing through the calibrator in the opposite order, this pattern minimises the impact of time variable instrumental errors (see Sect 5.2). Such errors were not included in our simulations, there were assumed to be effectively removed by having two opposite half cycles. Dwell times on calibrators were 30sec and the assumed antenna slew speeds 6deg/sec in azimuth and 3 deg/s in elevation. With these assumptions a full cycle took 7 minutes, of which approximately 2 minutes was spend slewing and 5 minutes integrating on source. Possibly somewhat shorter dwell times could be used. Generally 4 full cycles were assumed giving a total time for calibration of 28 minutes.

Fig 3 shows the result of using the above 5 calibrator observations and solving for cartesian coordinates and instrumental delay. An atmospheric outer scale of 1000m was assumed. The top row shows the results for baselines out to 500m while the bottom row shows results out to 10km. The left column of Fig 3 shows the x,y positions of where the LOS to the calibrators cuts the phase screen layers. For Fig 3 top left 10 layers were used there are 10 points per calibrator for each antenna, for Fig 3 bottom

left there are only two layers used. The most striking result of Fig 3 is that on all baseline lengths the rms on the z coordinate is at least a factor of 2 worse than the rms of x and y coordinates. The main effect that breaks the symmetry between z and x,y is that we only sample lines of sight over a hemisphere not a full sphere. Since there is a instrumental delay contribution we can only use delay differences to determine antenna positions. If we take the mean of the 4 horizon sources (to eliminate effects of x and y offsets) and subtract this from the zenith delay we get a quantity that depends on $\Delta z(1 - \sin(el))$. In contrast the y position is encoded in the difference delay between North and South sources and scales as $\Delta 2 \cos(el)$. I follows that for elevations of the horizon calibrators of 30° there is a much better 'lever arm' for determining x and y positions than for determining z positions.

Fig 3 top right shows show that for small baselines the rms on all cartesian coordinates increases at the 5/6 power of baseline length. This is the same power law dependence as is obtained for the rms phase versus baseline length when the atmosphere layer thickness is larger than the baseline (Treuhaft and Lanyi 1987). The reason is similar, in Fig 3 top left the control points to antenna 1 and those to antenna 2 have the same geometry as rays passing through a thick atmosphere, the mean separation between blue and red points is b, which is much less than $vT$ where T is the total length of the calibration observations. In this case the square root of the mean weighted sum of control point separations R to the 2/3 power (see Section 3) gives a 5/6 power law.

As the baselines get longer the x and y rms has a sharp saturation while the z error saturates more slowly. The saturation of x and y rms can easily be understood. The x term comes from comparing delays to the E and W calibrators. In Equ 15, the **F** elements have opposite sign for these observations, for long baselines the major contribution then comes from phase errors on a scale corresponding to the separation between the cuts of the E and W calibrators through the phase screen at the altitude ot 500m, which is of order 1000m. Hence the phase errors for x and y saturate at the values corresponding to separations in the screen of $\approx$ 1000m. In contrast for estimating the z components the **F** matrix elements are all positive for the cuts belonging to antenna 2 and negative for antenna 1, hence the phase contribution is always determined by separations in the screen equal to the baseline length. The importance of this different behavior for z and x,y depends on the atmospheric saturation length assumed. If this is 1000m as assumed in Fig 3 the differences are not dramatic, because even though for baselines > 1000m the z rms depends on the atmospheric delay difference within the screen for separations > 1000m, this itself saturates quickly due the small outer scale. In contrast for a larger saturation length the long baseline differences between x, y and z are more pronounced. Fig 4 illustrates what happens when the outer scale is 5000m, for $b > 1000m$ the x,y rms rapidly saturate, whereas the z rms scales as approximately $b^{1/3}$ when $1000m < b < 5000m$. Note that 'shoulders' seen in Fig 3 and 4 for the z -rms at 1000m are not artifacts but occur when the baseline length is comparable to the separation in x and y of the points which cut the turbulent layer. When this occurs for z there is a partial cancellation of points with opposite weights as defined in Equ 19 (in a plot like Fig 3 bottom left showing where rays intercept layers then at this particular baseline length some of the blue and red points almost exactly overlap)

An important question is how the rms errors on the coordinates scale with the total length of the calibration observation. On a baseline of length b it can be shown that the

spectrum of temporal phase errors correspond only to timescales from 0 to $b/v$, with the timescales on $b/v$ having largest amplitude. Phase fluctuations with timescales $> b/v$ are effectively eliminated by the phase differencing occurring across the interferometer baseline. The consequence is that for averaging times less than $b/v$ the rms of the mean phase increases with averaging time, whereas for averaging timescales significantly greater than $b/v$ the mean phase rms decreases statistically $\propto t^{-0.5}$. As expected we find that the antenna position simulations show similar behavior for the position rms vales. For x and y, as described above the maximum effective baseline is always 1000m, set by the separation of phase screen cuts to N and S calibrators, so for x and y for any calibration cycle time lasting longer than 100sec the rms decreases statistically. Since a single cycle takes about 7 minutes this effectively means that x,y position rms always scale statistically. This will nearly always be the case for z rms also, however in the case of a large outer scale of say 5000m, the characteristic time is of order 500sec, so that for a small number of cycles we find that the z rms on 5000m baselines decreases slightly slower than expected statistically.

We have seen that when solving for Cartesian coordinates and instrumental delay the z rms is much worse than the x and y rms. The main reasons for this is that we only observe over a hemisphere and are solving for the instrumental delay giving a smaller signal in the difference delays due to the z position offset compared to x and y. Another reason, which only affects long baselines, is the saturation in effective baseline length at the turbulent layer that occurs for x and y but not for z. When other geometrical parameters are solved for we find that these give further increases in the z rms. The reason is that other geometrical errors such as a non-intersecting axis offset ($\propto \cos(el)$) or a umodelled and different zenith dry delay at two antennas $\propto 1/\sin(el)$ are functions of elevation and are hard to distinguish from the signature of a z position offset which is also depends on elevation. The results of simulations of solving for extra geometrical parameters is given in Fig 5.

When solving for extra parameters more calibrators are needed and we have done tests with a 9 calibrator set (see Fig 5, top). It is found that a wide range of different elevations is essential, two sets of 4 horizon calibrators each with its own elevation does not allow a solution. There is obviously some possibility to optimise the calibrator distribution used, but the results in Fig 5 shows that as more parameters are solved for the z-rms gets very much worse while the x and y rms stays almost constant. The conclusion is that as much should be done as possible to remove the need for astronomical calibration of geometrical parameters (see Section 5).
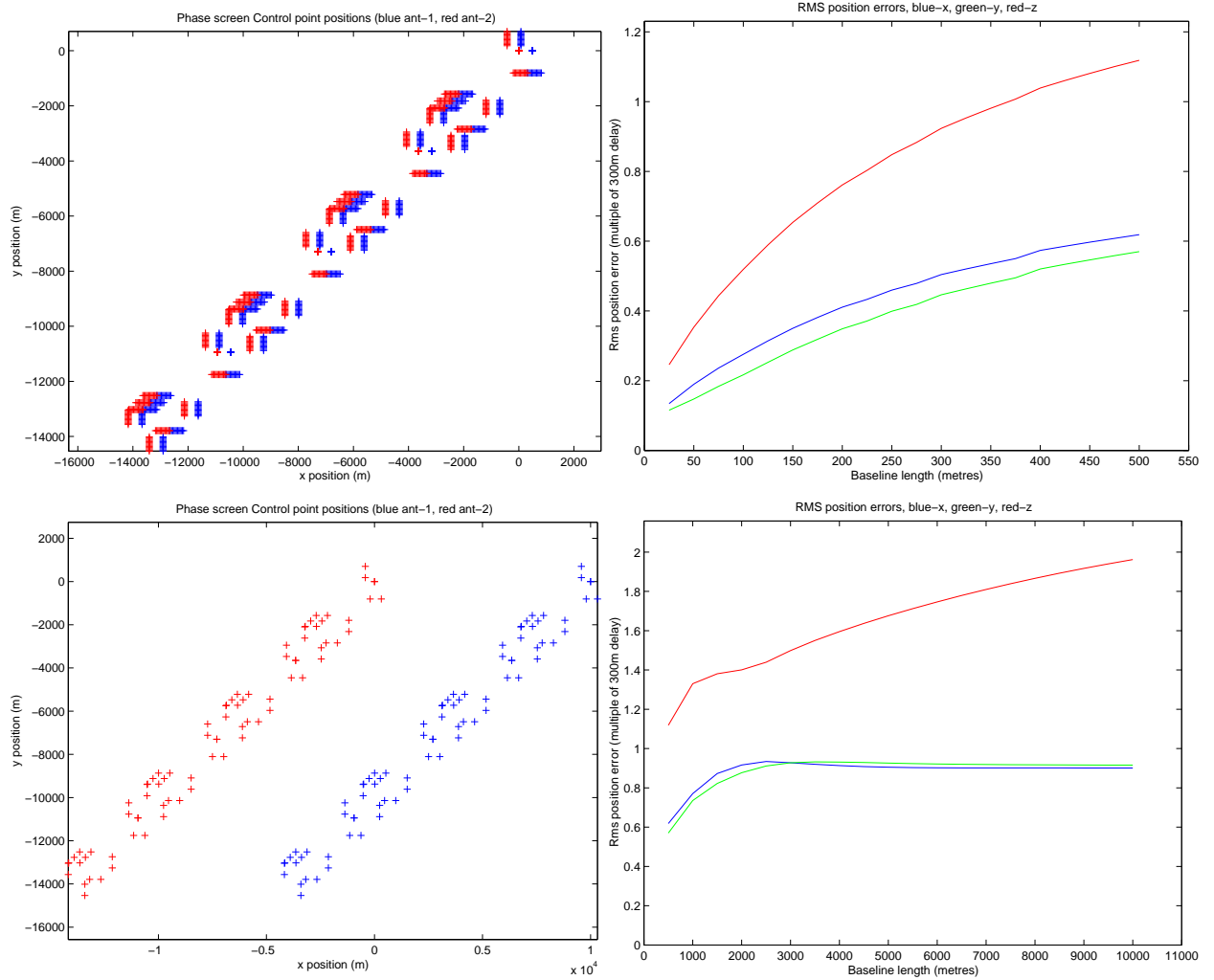
Figure 3: RMS errors on each component of the antenna position as a function of baseline length assuming an outer scale of 1000m. It was assumed that antenna cartesian position errors and an instrumental delay were solved for. A total of 5 calibrators were used, one at the zenith and 4 at N,S,E,W each 30° above the horizon. A full cycle consisted of a pass through these calibrators and then a pass in the opposite order, with dwell time on each calibrator of 30sec. Four full cycles were executed taking 28 minutes in all. **Top Left**, shows for baseline length of 500m, the places where the rays to each calibrator target cut the phase screen layers. Each calibrator observation has 10 points in a line corresponding to the 10 layers used. The red crosses are for antenna 1, while the blue are for antenna 2. **Top Right**. RMS errors on the Cartesian coordinates of antenna 2 versus baseline length out to 500m in units of the zenith rms delay on 300m baseline. **Bottom Left**. As for the figure at top left, except the baseline is 10000m. **Bottom right**. As for top right but for baselines out to 10000m.
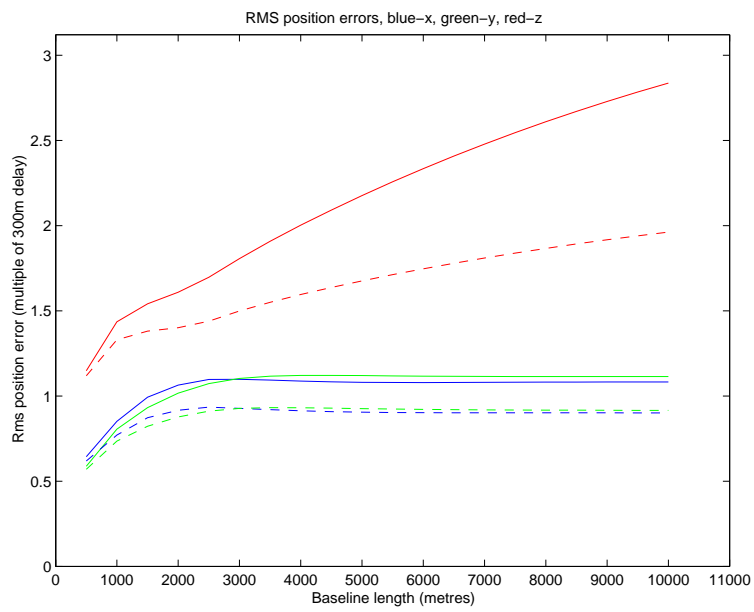
Figure 4: Effect of different outer scales. Parameters same as for Fig 3 except the solid line shows the rms errors on the Cartesian coordinates assuming a 5000m outer scale, while dashed line gives the result for an outer scale of 1000m for comparison
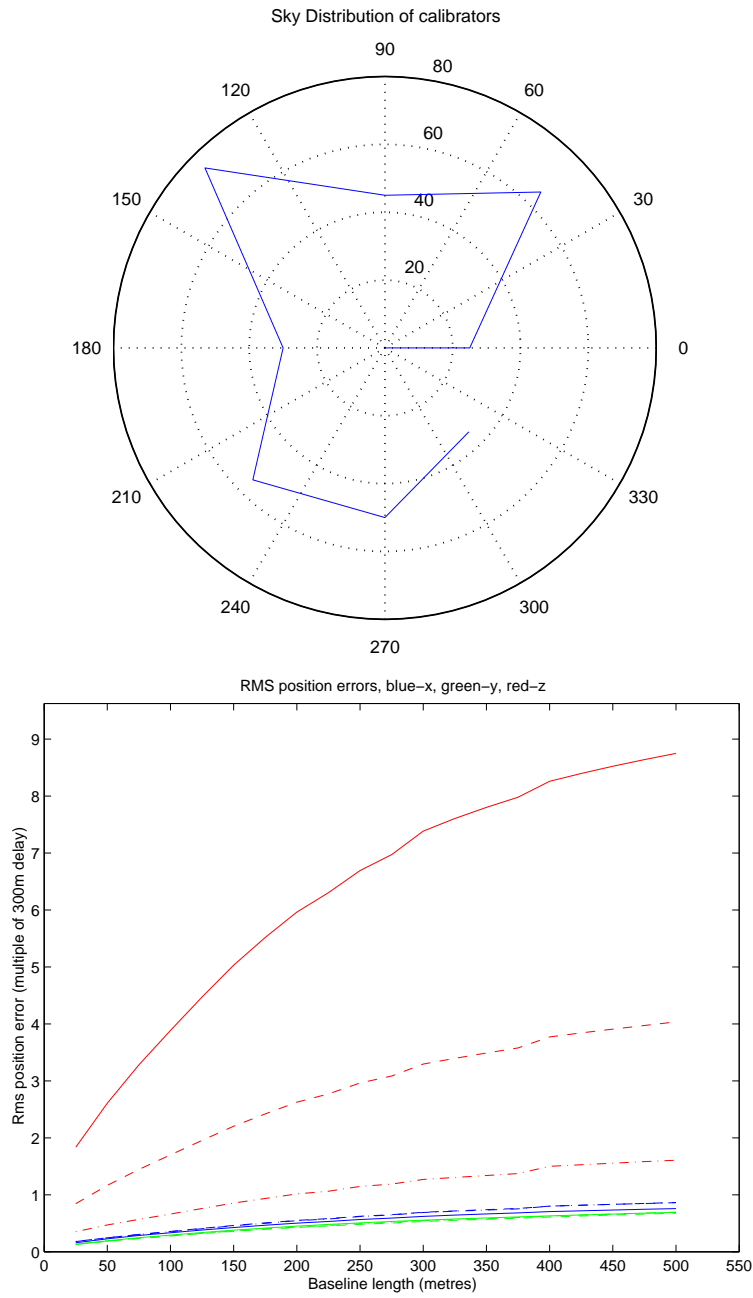
Figure 5: RMS errors as a function of the geometrical terms solved for. The observations used 4 cycles over 9 sources (25 minutes) and assumes an atmosphere outer scale of 1000m. **Top**. The sky coverage of the calibrators. **Bottom**. The rms errors on antenna coordinates. Solid lines- solving for Cartesian coordinates, instrumental delay, non-intersecting axis and dry delay. Dashed lines- solving for Cartesian coordinates, instrumental delay and non-intersecting axes. Dashed-dotted lines - solving for Cartesian coordinates and instrumental delay only.

# 8 Discussion and future work

This memo has outlined the procedures required to estimate antenna positions from astronomical observations and in particular has investigated the impact of the turbulent wet troposphere on the achievable accuracy. We have discussed the theory of single baseline calibration (Sect 3) and multiple antenna calibration (Sect 4.1) and evaluated the results numerically (Sect 7). There is still work to do, especially on evaluating in detail the realistic case of continuous reconfiguration where many antennas have good a priori positions and a few large position errors (see Sect 4.2). Despite these limitations we can now take a first look at whether achieving the proposed goal of $100\mu m$ rms relative position errors (Holdaway et al 2001) is realistic.

## 8.1 Compact array

Section 7 shows, unsurprisingly, that the limitations from the atmosphere on position location are very baseline length dependent. Consider first the most compact array, which has the highest demands on position accuracy because it will presumably be doing a large fraction of the THz astronomy. Assume starting from initially totally unknown antenna positions and using full array calibrations so that the analysis of Sect 4.1 can be applied. Sect 4.1 shows that the rms error on relative separation depends on the baseline length and is the same as if these two antennas conducted their own independent single baseline calibration. For a maximum antenna separation of 150m, assuming (from Fig 2) median nighttime conditions of rms delay $150\mu m$ on a 300m baseline, then Fig 3 suggests in 30minutes a z -rms of $97\mu m$. In this small baseline regime the simulations (see Section 7) show that rms error reduces statistically with solution time so in 2 hours a z-rms of $48\mu m$ could be achieved. It seems likely therefore that the stochastic atmosphere will not be a limitation on achieving the proposed goal for the most compact array or even those out to 500m maximum baseline.

## 8.2 Intermediate Configurations

When we consider the intermediate sized configurations of ALMA estimating the achievable accuracy is more difficult. A significant problem is our lack of knowledge of the outer scale of the turbulence (see Sect 6 and Fig 4). In addition the continuous reconfiguration makes analysis more difficult (see Sect 4.2). Intermediate arrays will be formed by moving 4 antennas at a time on average every 2.5 days. We propose doing the calibration of these intermediate arrays in two phases. First immediately after being moved, and completing initial pointing calibration by late afternoon there will be a first position calibration. Later on in the middle of the night a more accurate calibration will be done. The initial calibration will in outward reconfiguration use method 3 (see Sect 1) and in inward reconfiguration method 5. This calibration will last for 30 minutes and involve using 4 additional antennas from the array. These 4 antennas will be the ones moved in the previous reconfiguration. The second calibration in the middle of the night will use all antennas (cal method 1) for 60 minutes or so.

Using a 'full array' calibration for the main calibration seems the right strategy for a number of reasons (1) To avoid the rapid accumulation of errors if the other method are used repeatedly. (2) It allows antennas to be involved in many cal runs between the

times when they are moved, allowing a statistical reduction in their position errors. At any given configuration different antennas will have been involved in between 1 and 16 such cal runs depending on their position in the array. (3) For large arrays it allows the solution of systematic horizontal delay gradients with little extra overhead and little increased rms error (see Section 5.4).(4) It allows monitoring in possible drifts in positions due to soil changes etc. (5) It can be combined with other necessary calibrations such as for bandpass. A 1 hour session every 2.5 days or 60hrs amounts to almost 2% of the total ALMA observing time for position calibration, however it will be a higher fraction ($\approx 5\%$?) of periods of good phase stability.

Unfortunately a proper method of analysing the antenna position errors in the case of continuous reconfiguration has not yet been developed (see Section 4.2). A upper limit to the delay errors on all baselines can be provided by assuming we did full array calibration for 1 hour with initially no knowledge of the positions (see Sect 4.1). However as noted above the average antenna will actually have been involved in 8 hours of such calibrations and will have considerably better positions. It is clear that there will be a considerable range in antenna rms error depending on where in the array it is and how long it has been since it was moved.

In Table 2 we attempt to give some estimate of rms errors in different intermediate sized configurations. We give estimates of 'typical' errors for a given array by calculating from the simulation in Section 7 the expected z component error for the median length baseline in each configuration (see Fig 6), assuming a total integration time of 8 hours. The last number takes account of the fact that the average antenna will have been involved in 8 times 1 hours of calibration. We assume the atmospheric outer scale is 1km. Again median nighttime phase stability is assumed. Also listed are maximum errors in the case of outward reconfiguration. These maximum errors will apply to baselines involving the newly placed antennas. These antennas will have only been involved in 1 hour of calibration observations. We assume that the position solution between the moved antenna and the others with well known relative position will be dominated by the shortest baselines to this moved antenna (which for outward reconfiguration is given in Fig 6). Finally we also give an estimate of the errors to these just moved antennas after the initial daytime calibration.

The results in Table 2 shows that the initial position calibration of the moved antennas done in mid afternoon can be large. In the worst conditions the errors may be as large as 2mm. Under such conditions it might not even worth doing an astronomical calibration. In order to ensure that any antenna positions corrections can be applied retroactively this means that all data (even those observed in continuum mode) must be stored with a minimum number of spectral channels. A 3.6cm position offset will produce a one turn phase change over the 8GHz bandwidth. A 2mm position error therefore produces a 20° change over the same frequency range. A phase change of $\Delta\phi$ radians over a spectral channel causes a coherence loss in amplitude of $\Delta\phi^2/12$. If the data were averaged over the full 8GHz there would be a loss of 1% in amplitude. Storing the data as 8 frequency channels would reduce the loss by a factor of 64. For such 8 channel storage (i.e 1GHz spectral channels) the position error would have to be 5mm to produce a 0.1% amplitude and sensitivity loss.

## 8.3 Self-calibration

Table 2 shows that after the nightime calibrations the the mean errors can be kept below the target even out to the largest Y+ configuration. In contrast the largest errors can be several times the proposed target. Is this a serious concern? As noted in the introduction the present target is somewhat arbitrary, the effect of increasing antenna position induced phase errors is to gradually limit the dynamic range (and astrometric accuracy, see below) of images made from fast switching. One rational approach to setting targets for external calibrations is to set them so that noise limited images of sources of all brightness can be made. The limits should be set so that weak sources, requiring limited dynamic range, can be imaged purely by fast switching. Brighter sources when imaged by fast switching will be limited in dynamic range but for these sources there is enough SNR per solution interval that self-calibration can be employed. If the target for a priori calibration is set too low there will be a range of intermediate brightness sources in which noise limited images cannot be made by either pure fast switching or (fast switching plus) self-cal. It can argued that the a priori calibration requirements should rationally be set so there are no ranges of source brightness for which we cannot obtain noise limited images. In fact it can be argued that for imaging the a priori calibration accuracy need not be much better than this limit.

Antenna position errors are particularly suited for solution by self-cal because they introduce only between 1 and 4 unknowns per antenna over the whole source observation period. The first limit applies in the case of short tracks (or all expts when z errors dominate) the second in the case of long tracks where we must solve for all three Cartesian coordinates plus instrumental phase. Only relatively few parameters must be solved for and the solution time is long; the whole source observation period. Roughly speaking provided the initial image using pure fast switching has a limited dynamic range due to antenna position errors better than 20:1 then it seems there should be enough SNR per baseline to use self-cal to remove antenna position induced effects, and allow noise limited imaging of all sources. It can be objected that if the source is heavily resolved the SNR on the longest baseline will not be sufficient for self-cal, but then it will not be needed because the SNR is low and the antenna position errors from these baselines contributes very little to the errors in the image.

Self-cal of course does not help in astrometry projects and astrometric requirements could be used to set the goals for antenna position calibration. The difficulty is that serious astrometry projects would probably employ (as is done in VLBI) multiple calibrators surrounding the target source (or a weak 'secondary' calibrator very close to the target) to eliminate residual errors due to antenna positions and other errors. Analysing all these strategies would be time consuming.

## 8.4 Specifications and future procedure optimisation

In a sense setting a hard specification for the accuracy of antenna position may not be the most useful approach. We have a limited time to give to antenna position calibration and ultimately the achievable accuracy is limited by the atmosphere over which we have no control. The most important immediate goal of this memo is to ensure that the specifications on the hardware and software, which we do control, are sufficient to allow accurate antenna position calibration. We come to the following

conclusions

### 8.4.1 Hardware Specifications

(1) In order be used to recover turn ambiguities in the phase, changes in bandpass phase and IF delay induced phase differences over a 8GHz bandwidth of less than 8° over 3 days are required. This corresponds to a limit of changes of IF delay over this period of less than 2800fsec.

(2) The present specification on short time delay stability of 22fsec in 300 sec seems to be sufficient for the purposes of antenna position calibration.

(3) Adding a method of continuously monitoring the instrumental delay could halve the rms position errors.

(4) A network of sensitive barometers (0.1mb accuracy) distributed at the perimeter and centre of the site would be useful for reducing the delay and phase effects of horizontal pressure gradients. Such ancillary data can be used for correcting target source data from fast switching observations, and also during antenna position calibration observations. For the latter observations linear delay gradients can also be solved for as part of the antenna position determination process if a significant number of antennas are used for calibration.

### 8.4.2 Software Specifications

(5) To ensure no loss of amplitude and sensitivity due to phase coherence losses induced by uncertain antenna positions, all data, even continuum, should always be stored with multiple channels, each with width < 1GHz.

(6) On an antenna move day final pipeline processing of data may have to be postponed by up to 12hours; to allow the effect or updated antenna positions to be included in the imaging process. Subsequent re-running of the pipeline should be possible even later in rare cases where high dynamic range imaging requires the use of the latest estimates of antenna positions.

### 8.4.3 Procedure/Operations Specifications

(7) For optimising the recovery of phase turn ambiguities and to be relatively insensitive to weather a low frequency should be used for the antenna position calibration, 90GHz seems optimum.

(8) An antenna calibration will consist of several cycles through between 5 and 9 bright calibrator sources well distributed over the sky. A full cycle will consist of two half-cycles in opposite order through the calibrators (to reduce the effects of temporal drifts in instrumental phase). A full cycle will take between 7 and 11 minutes, a minimum of three full cycles should be executed to eliminate bad data.

(9) The main antenna position calibration will be done at night after an antenna move, will use all antennas and last 30 - 60 minutes. A preliminary calibration for 30 minutes will be done in late afternoon after the antenna moves have been made.This calibration

|                                | Config 9 | Config 18 | Config 27 | Largest Y+ |
|--------------------------------|----------|-----------|-----------|------------|
| Median baseline length (m)     | ≈150     | ≈400      | ≈1400     | ≈10000     |
| Median baseline error          | 26       | 37        | 52        | 75         |
| Max baseline error(night)      | 120      | 195       | 210       | 225        |
| Max baseline error(daytime)    | 480      | 780       | 840       | 900        |

Table 2: Estimates of rms baseline errors on different sized configurations (in microns). The first row gives errors on median length baselines. The second row the estimated errors on the just moved antennas to all other antennas after nightime calibration (assuming outward reconfiguration, the errors to just moved antennas will be significantly less for inward reconfiguration). The bottom row shows the errors to the same antennas after the initial daytime calibration. Median nightime and daytime phase stability is assumed. Also assumed is an atmospheric outer scale of 1000m and that only Cartesian coordinates and instrumental delays are solved for. The errors for the largest Y+ array may increase by a factor of 1.5 if the wet troposphere outer scale is 5km.

will involve the 4 moved antennas and the 4 antennas who were moved in the previous reconfiguration (since these give short baselines).

Beyond checking the specifications on the hardware and software we can in future attempt to further optimise the calibration procedure. Defining this procedure is of course important for planning the array operations. Knowing what can be achieved may also affect what science is planned in each array. We might in future pose the question of antenna position calibration by asking what is the optimum procedure in any given array given some fraction of the baseline-hours ($< 5\%$) can be allocated to position calibration? What then is the achieved accuracy in each configuration? Finally, at what frequencies will this be sufficient to allow noise limited images of sources of all brightness to be made, using either pure fast-switching or fast switching plus self-cal?

# Software

The matlab software used in generating figure 3,4,5 and for making the estimates of achievable position accuracies will be placed at

`http://www.oso.chalmers.se/~jconway/ALMA/SOFTWARE/index.html`

# References

ALMA Antenna Specification 2004, Sect 5.2.5. 'Antenna Alignment Specification'
Bacmann, A., Guilloteau, S., 2004, ALMA memo in prep (draft of as July 28th 2004 at `http://www.cv.nrao.edu/%7Eawootten/mmaimcal/bandpass_memo.pdf}`).
Butler, B., Holdaway, M.A,, Wootten, A., Lucas,R. Magum,J.G., 2004, SCID-90.03.00-007-A.PLA, Draft 2004-02-27
(`http://almaedm.tuc.nrao.edu/forums/alma/dispatch.cgi/ipt90docs/docProfile/100102/d2004`
Beasley, A., Conway, J.E., Nyman, L-A., Holdaway, M., 1997, AA, 124, 469.
Carilli, C.L. Holdaway, M.A., 1999, ALMA memo 262.
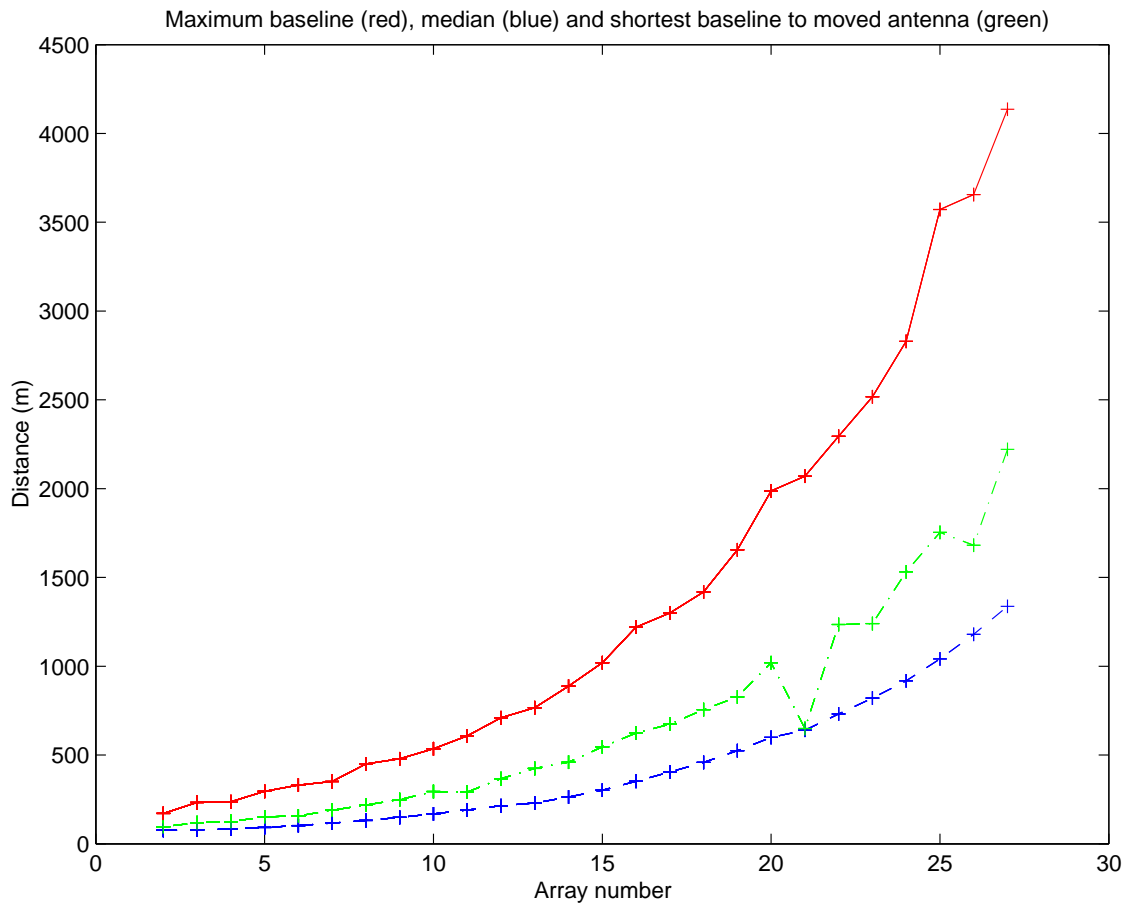Chen, G., Herring, T.A., Journal of Geophysical research, Vol 102, No B9, 20489.

Figure 6: Size of baselines as function of configuration number. Red shows the maximum baseline, blue shows the median length baseline and green the distance from each of the newly occupied pads (in outward configuration) to the nearest occupied pad. Note this diagram does not show the Y+ part of the array which has maximum length baselines extending to 19km.

Delgado. G., 2001, ALMA memo 361

Holdaway, M.A., Wootten, A., Payne, J., Vaccari, A., Emerson, D, Mangum, J., 2001, Calibration Specifications and Requirements, ALMA-90.03.00.00-001-A-SPE

Holdaway, M.A., Radford, S.J. Owen.F.N., Foster, S.M., 1995, ALMA memo 129.

Hills, R, Richter et al 2004, 'Ancillary Calibration Instruments' document in prep, SCID-90.05.13.00-001-A-SPE

Ishimaru, A. 1997, 'Wave Propogation and scattering in random media', IEEE press series on electromagnetic wave theory, IEEE/Oxford Univ. Press classic reissue.

Robson. J., et al, 2001, ALMA memo 345.

Sramek, R., 2004, 'ALMA System Technical Requirements', ALMA-90.04.00.00-005-A-SPE

Treuhaft, R.N., Lanyi, G.E., 1987, Radio Science 22(2), 251.

Wright, M., 2002, ALMA Memo 427